Nanopore Fabrication Made Easy: A Portable, Affordable Microcontroller-Assisted Approach for Tailored Pore Formation via Controlled Breakdown

Y. M. Nuwan. D. Y. Bandara[1,*], Buddini I. Karawdeniya[2], Shankar Dutt[3], Patrick Kluth[3,*], and Antonio Tricoli[1,4*]

[1]Nanotechnology Research Laboratory, Research School of Chemistry, The Australian National University, Canberra, ACT, Australia

[2] Department of Electronic Materials Engineering, Research School of Physics, The Australian National University, Canberra, ACT, Australia

[3]Department of Materials Physics, Research School of Physics, The Australian National University, Canberra, ACT, Australia

[4]Nanotechnology Research Laboratory, School of Biomedical Engineering, Faculty of Engineering University of Sydney, NSW, Australia

*Corresponding Authors: nuwan.bandara@anu.edu.au, patrick.kluth@anu.edu.au and antonio.tricoli@sydney.edu.au

Keywords: Nanopore Fabrication, Controlled Breakdown, Arduino, Low-cost fabrication, Single-molecule sensing

Abstract

With growing interest in solid-state nanopore sensing—a single-molecule technique capable of profiling a host of analyte classes—establishing facile and scalable approaches for fabricating molecular-size pores has become increasingly important. The introduction of nanopore fabrication by controlled breakdown (CBD) has transformed the economics and accessibility of nanopore fabrication. Here, we introduce the design of an Arduino-based, portable CBD device, with an estimated cost of <150 USD, which is >10-100× cheaper than most commercial solutions, capable of fabricating single nanopores conducive for single molecule sensing experiments. We demonstrate the facile fabrication of 60 tailored nanopores with ~80% of the pores (~2.5-12.6 nm) within 1 nm of the target diameter. Selected pores were then tested with double-stranded DNA, the canonical molecular ruler, demonstrating their performance for single-molecule sensing applications. The device is constructed with off-the-shelf readily available components and controlled using a highly customizable MATLAB application, which has capabilities encompassing pore fabrication, pore enlargement, and current-voltage acquisition for pore size estimation. When combined with a portable amplifier, this device also provides a fully portable sensing platform, an important step towards portable solid-state nanopore sensing applications.

Introduction

A nanopore is an aperture through an otherwise impervious membrane that function as the sole fluidic pathway between two electrolyte reservoirs with applications including the detection and characterization of biomolecules/particles such as DNA, proteins, glycans, liposomes, and viruses.[1-6] While the dawn of nanopore-based single molecule sensing is linked to biological nanopores,[7, 8] solid-state nanopores (SSNs) started gaining significant interest in the last two decades, due to numerous benefits they offer such as tunability in pore size and, surface chemistry, and compatibility across a wide chemical and physical conditions. The membrane material composition has expanded beyond the initial polymer

materials such as polycarbonate and polyethylene terephthalate[9-11] and silicon-based materials such as silicon nitride (SiN_x)[12] to 2D materials like graphene.[13, 14], h-BN (hexagonal boron nitride)[15], MoS_2 (molybdenum disulfide)[16, 17], and, WS_2 (tungsten disulfide)[18]. A driving force behind this expansion in material composition is the increasing interest in sequencing, whether it pertains to DNA or proteins. Additionally, there is a growing exploration of metal-based materials such as HfO_2[19], MOFs (metal-organic frameworks)[20], TiO_2[21], and, ZnO[22]. Unlike natural nanopores that typically (self-)assemble from a lipid bilayer, pores in solid-state membranes are generally fabricated top-down, which can limit the overall throughput of the technology and the accessible size range. Single pore fabrication was initially mainly carried out using microcopy-based methods such as transmission electron microscopy (TEM) and focused ion beam microscopy (FIB).[12, 23, 24] This enabled the fabrication of pores in the order of a few nanometers in diameter with TEM up to a few hundred nanometers with FIB. During the early stages of solid-state nanopore sensing *Li et al* pioneered the shrinking of pores via ion-beam sculpting[12]. However, these fabrication methods are expensive, require highly trained users, and have often low throughput. Moreover, since the pore is not fabricated in its native sensing environment, *fabrication-to-sensing* requires multiple transfer steps that can lead to membrane fracturing. Thus, the development of affordable and efficient membrane and nanopore fabrication methods is crucial for the widespread adoption of solid-state nanopore technology.

The advent of controlled breakdown (CBD) technology[25] has made nanopore fabrication affordable, efficient, and cost-effective. This is also leading to the emergence of a family of *sister* fabrication technologies such as laser-assisted controlled breakdown[26], multi-level pulsed voltage injection[27], tip-assisted localized breakdown methods[28, 29], tesla-coil assisted breakdown[30], and, chemically-tuned controlled breakdown (CT-CBD).[31, 32] While the initial demonstration of CBD was performed with Si-rich SiN_x membranes, fabrication of pores through other materials such as near stoichiometric SiN_x[33], HfO_2[34], graphene[35], MoS_2[36] has also been demonstrated. Notable work has also been done to address key initial reservations associated with CBD technology. For example, to counter the skepticism surrounding

the formation of multiple pores rather than a single pore, a thorough investigation of electrical and solution conditions in tandem with DNA as a molecular ruler was conducted enabling to identify the limits of the CBD method and suboptimal process conditions. It is advisable to use electric fields <1 V/nm for initial pore formation and during the pore enlargement phase, no more than half the voltage used for initial pore formation to be used[37]. The CBD sister technologies are also not immune to multiple pore formation. *Goto et al* showed the formation of multiple pores resulting from an unoptimized multi-level pulsed voltage injection method[38]. The *soft breakdown* phenomenon, resembling the formation of a pore but arising from the formation of a conductive pathway with incomplete removal of material,[39] should also be avoided. With growing interest in the fabrication of smaller diameter pores for small molecule sensing and sequencing, *Briggs et al* reported a CBD-based protocol to fabricate sub-2 nm diameter pores along with strategies to overcome initial rectification associated with such smaller pores[40]. *Waugh et al* have provided a detailed account of the CBD process, instrumentation, and software control to fabricate low-noise and size-controlled pores[41]. While legacy issues associated with nanopores (not limited CBD) have precluded nanopore operations lasting several hours, more recently, *Dutt et al* achieved >1.5 million detection events, using CBD with BSA as the analyte.[33] *Saharia et al* further pushed the boundary of sensing even further with ~2 million DNA events using a well-optimized CT-CBD protocol yielding ultra-stable current over several hours[31].

While the primary custom circuitry used for the CBD process is affordable (<100 USD), they are often connected to a block connector and a data acquisition (DAQ) system, which cost several thousands of dollars and upward. While these electronic components are still far less costly compared to microscopy-based methods, the barrier to adoption could be further reduced by a design strategy employing readily accessible parts which could also play a key role in commercialization efforts as well. To this extent, we chose an Arduino Uno-based platform to develop a portable and low-cost CBD device. Arduino microcontrollers are widely available, affordable, and rugged hardware with vast online community support. While Arduino microcontrollers have been used in various capacities for pore fabrication setups,

they are typically used as a regulator/switch in most cases. For example, *St-Denis et al* used an *Arduino Due* in a tip-controlled pore fabrication protocol to control the current flow across the pore.[42] *Fang et al* used an Arduino microcontroller in their fabrication protocol with transient high electric fields to regulate the voltage pulse used for nanopore formation.[43] Similarly, *Kuan et al* used an Arduino controller for pulse triggering in their protocol to fabricate graphene nanopores.[44] However, in most cases, the Arduino microcontroller is used in consort with other benchtop devices.

Here, we introduce an Arduino-based device design for nanopore fabrication via CBD; a custom-MATLAB application was developed to control the outputs of the Arduino-based device where an electric field <1V/nm is applied across the membrane to form a single nanopore. Overall, 60 pores with sizes ranging from ~2.5 to ~12.6 nm were fabricated through ~10 ± 2 nm thick Si-rich silicon nitride membranes. Moreover, ~80% of the fabricated pores were within 1 nm of the target pore diameter. The fabricated nanopores were then used to translocate double-stranded DNA where characteristic resistive pulses were observed. The overall cost of the device is <150 USD which could potentially facilitate the widespread adoption of CBD technology for nanopore fabrication and by extension the expansion of SSN sensing technology.

Experimental

Device Development: All parts used for the Arduino-based CBD device are listed in Table 1.

Part Name	Supplier	Part Number	Quantity	Total Price (USD)
Arduino UNO Board	eBay	Freenove	1	17.29
12-bit External DAC	Core Electronics	DFR0552	1	5.74
AD820 OP-AMP	Digi-Key	505-AD820ANZ-ND	3	26.43
12V Boost (only for breadboard implementations; *vide infra*)	Core Electronics	POLOLU-4016	1	11.35
Voltage Display	eBay	201313168179	1	6.61
Dual Power supply	eBay	155104110631	1	12.73

1 MΩ resistors	Digi-Key	A105943CT-ND	7	4.00
5 MΩ resistor	Digi-Key	SM102035004FE-ND	1	4.58
10 MΩ resistor	Digi-Key	BC10.0MZTR-ND	1	0.33
ADS-1115	eBay	303971402874	1	8.81
100 nF Capacitors	DigiKey	1010-1204-ND	4	9.13
47µF Capacitor	eBay	284828430018	1	0.01
Header Connector (6 positions)	Digi Key	732-2859-ND	1	0.75
Header Connector (10 positions)	Digi Key	S7004-ND	2	1.11
Header Connector (Male)	Digi Key	10129378-910003BLF-ND	3	0.90
DIP 8 Socket	eBay	2.84579E+11	3	1.38
PCB Board	PCBWay	-	2	26.16
Total				136.87

Table 1: Details about the parts used for the Arduino-based CBD device. Prices were computed using the average exchange rate (Australian Dollar to United States Dollar) for 2023 (January to April).

Communication Protocols: The Arduino microcontroller was programmed using the MATLAB *Appdesigner* platform (SI Section 1). Coding to communicate with I^2C devices through MATLAB may not be as straightforward as with the native Arduino programming environment. SI Section 2 provides key lines of codes that are crucial for successful communication with the two I^2C devices used in the design. The MATLAB code for the GUI is available through https://github.com/ssnl-anu/poremaker. We believe since both Arduino and MATLAB are popular platforms, the availability of the schematics and programming code would propel the advancement of this device class even further to create more sophisticated products (i.e., low noise and for wider adoption of the CBD technology).

Arduino Board: Some Arduino boards are clone boards with a CH340 USB chip and require manual installation of the CH340 driver. The Arduino board listed in Table 1 is a plug-and-play device.

Furthermore, it has a more amicable USB-C type socket instead of the typically seen USB-B type socket. SI Section 3 discuss about other hardware selection considerations.

Solution Preparation: 1M KCl was prepared by dissolving the solid (Sigma-Aldrich, P9333) in 18 MΩ.cm ultra-pure water. The pH and the conductivity of the buffered KCl solution (10 mM tris and 1 mM EDTA, Sigma-Aldrich, PPB010) were measured using the Orion Star™ pH meter. The KCl solutions were then filtered using Millipore Express® PLUS PES filters of 0.22 µm pore size. This KCl was used for both nanopore fabrication and DNA translocation experiments.

Nanopore Size Estimation: A current-voltage (I-V) curve was obtained using the *eNPR-100 kHz* amplifier or *eNPR-10MHz* amplifier by sweeping the voltage from -200 mV to +200 mV. The slope of the curve (i.e., open-pore conductance, G) was then used to estimate the diameter of the pore using,

$$G = K\left(\frac{4L}{\pi d^2} + \frac{1}{d}\right)^{-1} \qquad \text{Eq. 1}$$

K, L, and d are solution conductivity, membrane thickness, and pore diameter.

DNA Translocations: All DNA experiments were carried out in 1M KCl buffered at pH ~8. DNA (1kb, Thermo-fisher SM0311) using the Elements 100 kHz amplifier. The DNA is added to the *cis* side (~0.7 µg/mL), and +400 mV is applied to the *trans* side to translocate the DNA electrophoretically across the nanopore. Data were acquired at a sampling rate of 100 kHz and lowpass filtered at 10 kHz. All events were extracted using the *EventPro* (3.0) platform.[45]

Results and Discussion

The breakdown of the total cost of the Arduino-based device is shown in Table 1. The proposed device costs <150 USD and is ideal for resource-limited settings. Moreover, it is portable and USB-powered. Figure 1 shows a schematic of the CBD device and the MATLAB-based interface used to communicate with the device. The chassis shown in Figure 1d was 3D printed in PLA (Bambu Lab P1P 3D Printer). Noise implications of this choice of material is discussed later. SI Sections 1 and 2 provide key

instructions for operating the MATLAB-based interface. While the native Arduino Integrated Development Environment (IDE) is often used to program Arduino microcontrollers, they (i.e., Arduino microcontrollers) are compatible with various other environments such as MATLAB, Python, and LabView. This provides excellent flexibility to the developer to customize their microcontroller depending on a host of factors such as application environment, cost, and expertise. In this work, we used MATLAB (with a graphical user interface, GUI) to control and view the microcontroller outputs since MATLAB-based applications are highly customizable and other users can incorporate custom fabrication protocols very easily using the MATLAB *Appdesigner*.

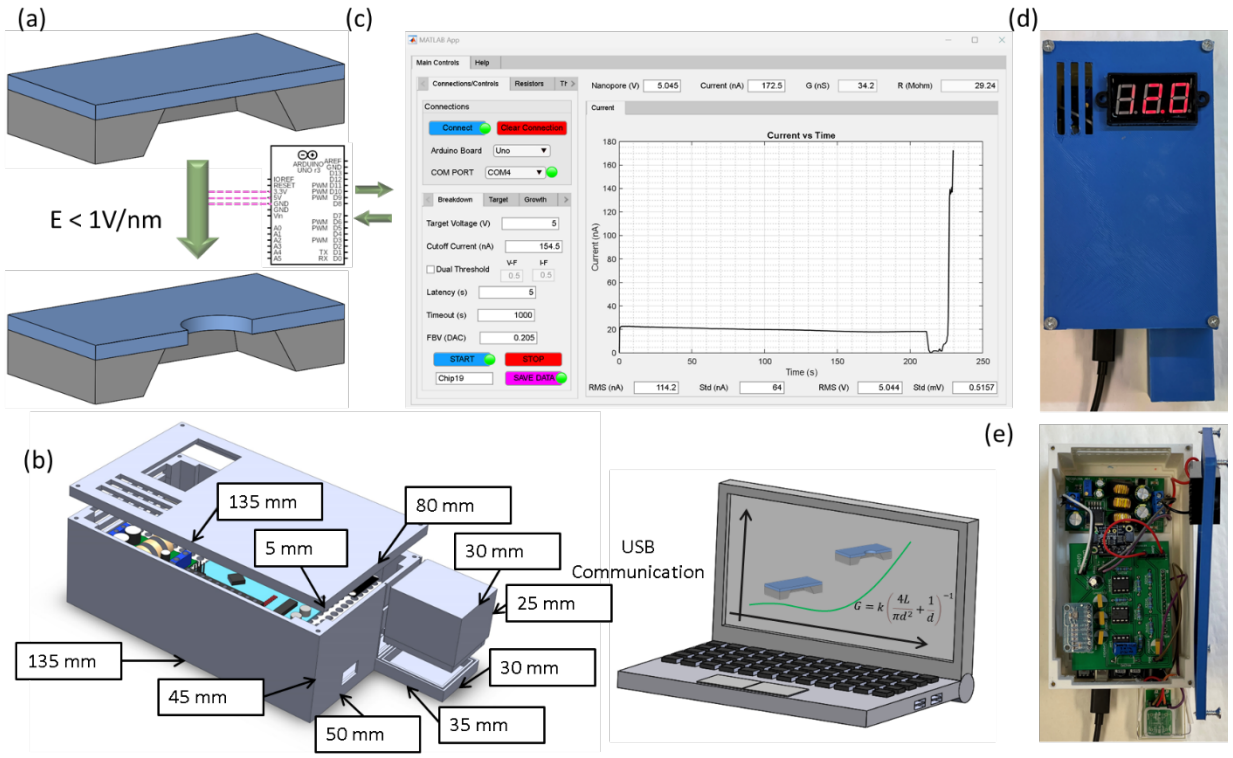

Figure 1: (a) Schematic of nanopore fabrication using our CBD device, where an electric field < 1V/nm is applied across the membrane. **(b)** CAD representation of the Arduino-based USB-powered device (with its dimensions). **(c)** MATLAB-based custom application. **(d)** and **(e)** Photographs of the device. More pictures of the device are shown in Figure S3. The compartment housing the nanopore chip was

specifically designed to fit flow cells from *Elements SRL.* Other flow cells can also be connected through the header pins that connect the electrodes to the PCB (Figure S4).

Addressing Limitations of the Arduino Board

The Arduino Uno board used in this design suffers from two major measurement resolution limitations: the absence of a DAC pin and the limited inbuilt ADC resolution (10 bits). Furthermore, the voltage output is limited to +5V which is not sufficient for most pore fabrication efforts. The following steps were taken to circumvent these limitations. SI Sections 3 and 4 provides detailed discussions of the device's electronic design strategy.

i) Since Arduino Uno doesn't have a DAC port, it resorts to pulse width modulation (PWM) to output the desired voltage: the voltage output is toggled between high logic (+5V, ON time) and low logic (0V, OFF time) to generate an averaged voltage output. Moreover, the resolution of the PWM pins is a mere 8-bits. The least significant bit (LSB)—the smallest interval that can be detected—is thus FSR/256, where FSR is the full-scale input range (5V for the Arduino Uno). An OP-AMP-based architecture can be used to convert the PWM pin to a DAC pin, as shown in Figure 2a. However, this PWM-OP-AMP-based DAC yields a noisy voltage output compared to the 12-bit external DAC (MCP4725) used in the design presented in this work, as seen in Figure 2a.

ii) The onboard ADC of the Arduino UNO has a resolution of 10-bits. An external 16-bit ADC module (ADS-1115) is used to improve the limited onboard ADC resolution of the Arduino (1 bit of this module is reserved for the sign of the voltage). The LSB improves from FSR/1024 to FSR/32768 with this approach. The ADS-1115 has a programmable gain amplifier (PGA), and it is by default set to ±4.096 (FSR of the ADS-1115). The measurement noise is also significantly reduced with the external ADC, as seen in Figure 2b.

iii) A DC-DC step-up boost converter was used to increase the maximum voltage output from +5V to ±24 V (Figure 2c). The +5V voltage output is not adequate to fabricate pores in relatively thicker membranes (e.g., >12-15 nm thick membranes). The boost converter was also used to power the dual-supply OP-AMPs as shown in Figure S2. The maximum output of the boost converter was limited to ±12V (which can be increased using the potentiometer of the module as shown in Figure S5) for safe operation of the AD820 OP-AMPs (maximum supply voltage is ±18V) and the external ADC (*vide infra*). The boost converter sometimes fails to register 0V at the negative output terminal soon after disconnecting power to the unit. Thus, the negative output terminal was grounded through a 47 µF capacitor as shown in Figure S2.

iv) Measurements at the external ADC are done differentially with respect to the ground. While the voltage applied to the OP-AMP #1 is measured directly, the current across the nanopore is measured through a resistor-capacitor arrangement, as shown in Figure S2. The measurements were unstable without such a resistor-capacitor arrangement.

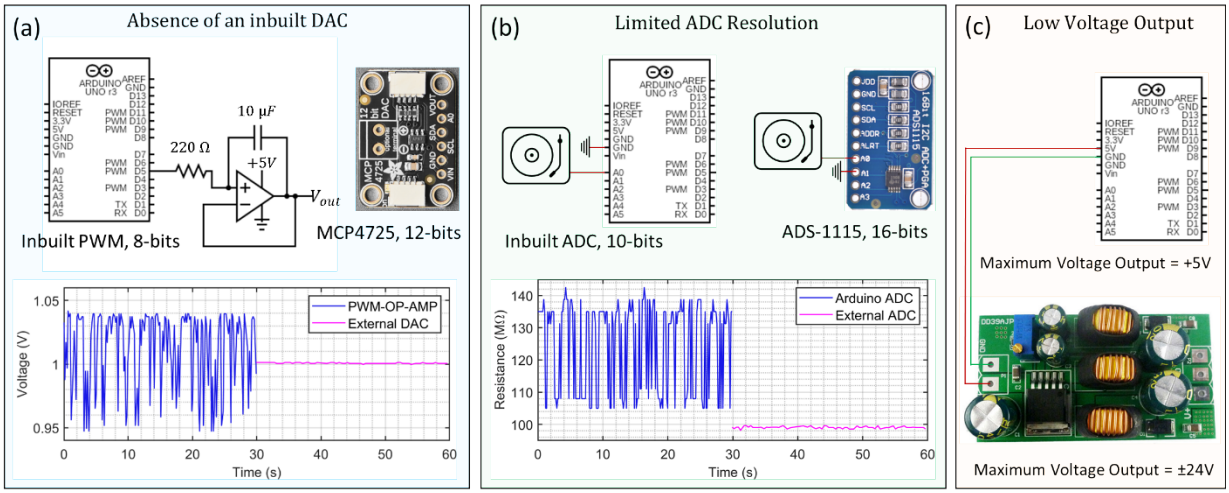

Figure 2: (a) Addressing the absence of an onboard DAC pin using an OP-AMP-based architecture or an external DAC (MPC4725): 30-second trace corresponding to 1 V output from the PWM- the OP-AMP configuration (blue trace) and the external DAC (magenta trace). **(b)** Addressing the limited resolution of the onboard ADC by using an external ADC (ADS-1115): 30-second trace corresponding

to the resistance of a 100 MΩ test resistor estimated through the in-built ADC of the Arduino (blue trace) and an external module (ADS-1115, magenta trace). **(c)** Addressing the seeming low maximum voltage output (for pore fabrication) by incorporating a DC-DC step-up boost converter to the design which can output up to ± 24V.

Device Performance

We used test resistors in the range of 1 GΩ - 1 MΩ (1 GΩ, 500 MΩ, 100 MΩ, 50 MΩ, 10 MΩ, 5 MΩ, and 1 MΩ) to mimic nanopores with conductance in the range of 1 nS – 1000 nS. For a cylindrical nanopore through a 10 nm thick membrane immersed in a solution of 1 M KCl with a conductivity of ~11.6 S/m, these conductances would translate to pores of ~1.1 nm - ~97.5 nm in diameter (evaluated using equation 1). Since the CBD method is best suited to fabricate ≲30 nm diameter pores, the boundaries represented by the test resistors cover and extend well beyond the resistances that would have to be measured with this device. Figure 3c shows the relationship between the expected and measured voltage from the device up to +12V. The dashed line represents a linear fit made to the data with a slope of 1.051 (ideally, the expected value is 1) and an R^2 value of 0.999. The upper voltage boundary can be increased using the potentiometer of the DC-DC step-up boost converter as shown in Figure S5. This upper voltage boundary (i.e., +12 V) was chosen because it is sufficient to fabricate pores through ubiquitously used ~10 nm thick membranes and limits the maximum voltage driven to the analog pins of the ADS-1115 to +3V (under the default PGA value). The resistance of each test resistor was calculated by taking an I-V curve and sweeping the voltage from 200 mV to 1000 mV in 10 steps, as shown in Figure 3d. The resistor values calculated from the slope of such I-V curves ($R_{measured}$) are shown in Figure 3e as a function of the expected resistance ($R_{expeced}$). The dashed line represents a linear fit made to the data with a slope of 1.022 (ideally, the expected value is 1) and an R^2 value of 0.999. Although not implemented in the current design, we have noticed the $R_{measured}$ values to be more stable when the connection point of the nanopore and the feedback resistor of OP-AMP #2 (Figure S2) are grounded through a 100 nF capacitor. This observation

intends to provide more context into improvements that can be made to the current design and for interested readers to pursue further. This can be easily implemented by inserting a 100 nF ceramic capacitor between pins 2 and 3 of the OP-AMP #2.

As noted previously, the chassis was 3D printed in PLA. While it may not provide best protection against electromagnetic interferences unlike with a metal chassis which acts like a Faraday Cage, the choice of material was not only due to the ubiquitous availability of 3D printers but also to be in alignment with the theme of the work—developing a device through readily available resources. However, it is imperative to look at the noise performance of the device since it (i.e., noise) can affect the overall performance of the device. Thus, we looked at current traces corresponding to the open circuit (i.e., no resistive element connected to the electrode leads) and close circuit (50 MΩ resistor to mimic a 20 nS pore) as shown in Figure 3f. A voltage bias of 1 V was used in Figure 3f. We looked at the standard deviation of a given trace (σ_I) as a metric of noise, where we did not see considerable change in σ_I with voltage (tested from 0-12V in 1V increments). Three times the average of the σ_I across the voltage range of 0-12V for each of the cases in Figure 3f ($\mu_{3\sigma_I}$) is shown in Figure 3h. As seen, the $\mu_{3\sigma_I}$ is less with the use of a Faraday cage (as expected): ~8% and ~17% improvement for open circuit and 50 MΩ (i.e., closed circuit) cases, respectively. Thus, placing the flowcell in a Faraday cage can improve the current design. However, given the magnitude of the noise values based on $\mu_{3\sigma_I}$ (<0.2 nA), the influence of this noise during pore fabrication is not significant within the pore sizes explored in this study. For example, if we consider the smallest pore fabricated with this setup (2.6 nm in diameter, ~12 nm thick membrane, 1M KCl, 10.85 S/m, fabrication voltage of 4.5 V, theoretical cutoff current of ~18.4 nA), the error in diameter from $\mu_{3\sigma_I}$ would be ~±0.01 nm.

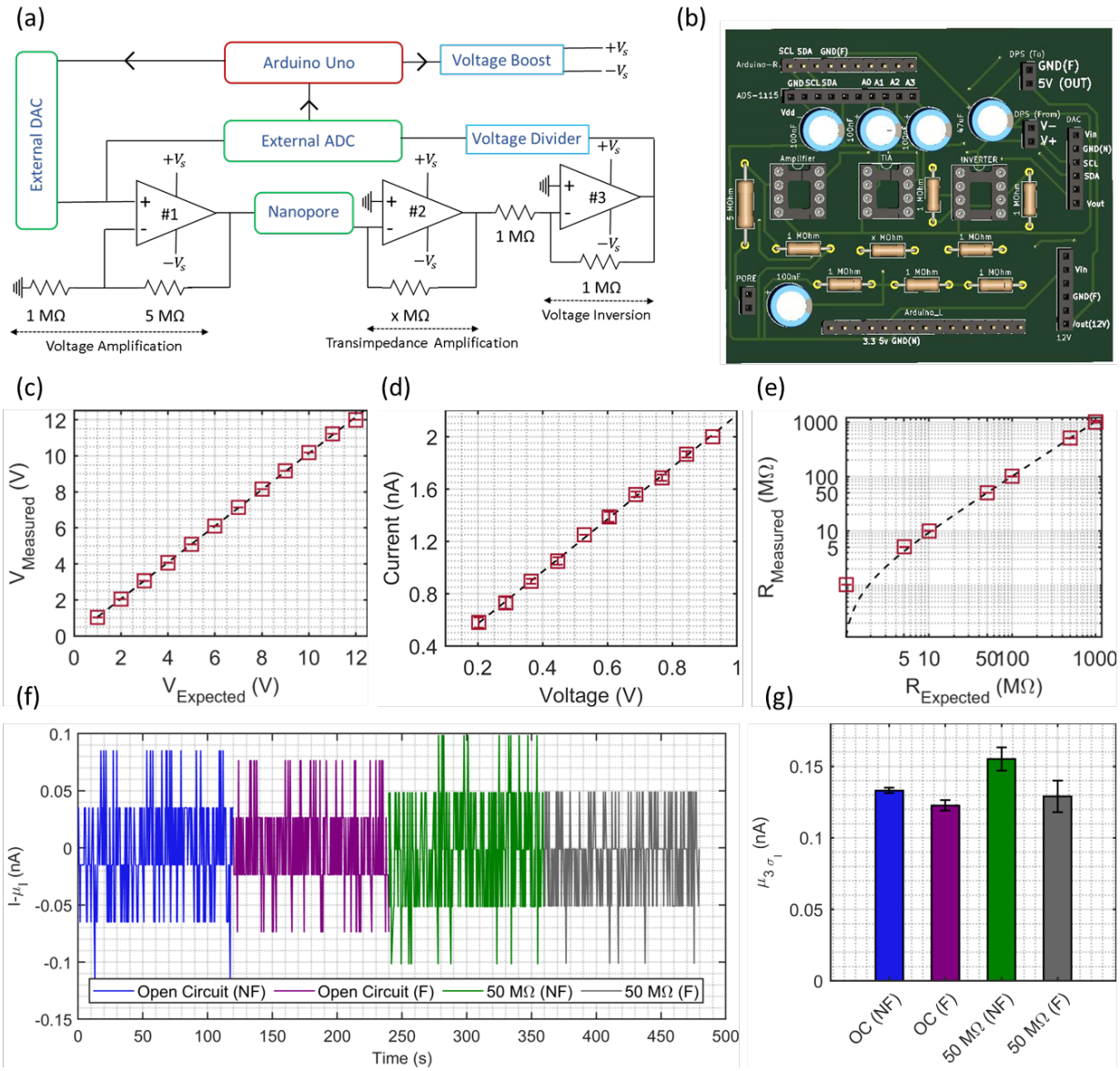

Figure 3: **(a)** Simplified circuit diagram of the pore fabrication setup (a more comprehensive circuit diagram is shown in Figure S2. **(b)** Printed Circuit Board (PCB) diagram of (a). **(c)** A plot of expected voltage ($V_{Expected}$) vs. voltage applied ($V_{Measured}$) from the pore fabrication setup (slope = 1.051 and R^2 = 0.999). **(d)** I-V curve corresponding to a 500 MΩ resistor (equivalent to a 2 nS pore). **(e)** A plot of calculated ($R_{calculated}$, evaluated using the slope of the I-V curve) and expected ($R_{Expected}$) resistance values for test resistors in the 1 GΩ - 1 MΩ range. The dashed line represents a linear fit made to the data (slope = 1.022 and R^2 = 0.999). **(f)** Mean subtracted current traces (under 1 V bias) corresponding to

open circuit without (blue) and with (maroon) placing the device inside a faraday cage (blue); 50 MΩ connected to the electrode leads without (green) and with (gray) placing the device inside a Faraday cage. **(g)** Mean of the three times the standard deviation of current traces obtained under applied voltages of 0-12V (in 1V increments) corresponding each of the cases shown in (f).

Nanopore Fabrication

Nanopores were fabricated through ~10±2 nm thick Si-rich silicon nitride (SiN_x) membranes with a SiO_2 underlayer[33] by applying an electric field <1V/nm across the SiN_x membrane. Figure 4 shows a flow diagram outlining the pore fabrication and the subsequent biomolecule translocation phase. In brevity, the knowledge of membrane thickness (either through the manufacturer or, for instances where membranes are fabricated in-house, the thickness can be assessed with an ellipsometer or a surface profiler)[33] and the chemistry of the solution that would be used for pore fabrication (mainly the conductivity and the pH) is needed to calculate the target diameter (d_{target}) using equation 1. In this study, pore fabrication was done using 1M KCl buffered at pH ~8. After determining the d_{target}, the electric field strength is set to be <1 V/nm. That is, if the membrane thickness is 10 nm, the maximum permissible voltage for pore formation is 10 V. However, the maximum electric field used in this study was 0.85V/nm. Furthermore, the minimum electric field used was 0.38 V/nm. A comprehensive list of electric fields used in this study can be found in table S2. While higher electric fields can lead to faster pore formation, they can also lead to larger-than-expected pore sizes. Although lower electric fields would slow the pore fabrication process, *Saharia et al*. have shown the benefits of resorting to lower electric fields for pore fabrication.[31] The breakdown voltage and the d_{target} would determine the cutoff current—the current threshold that would stop the voltage application across the membrane (*vide infra*).

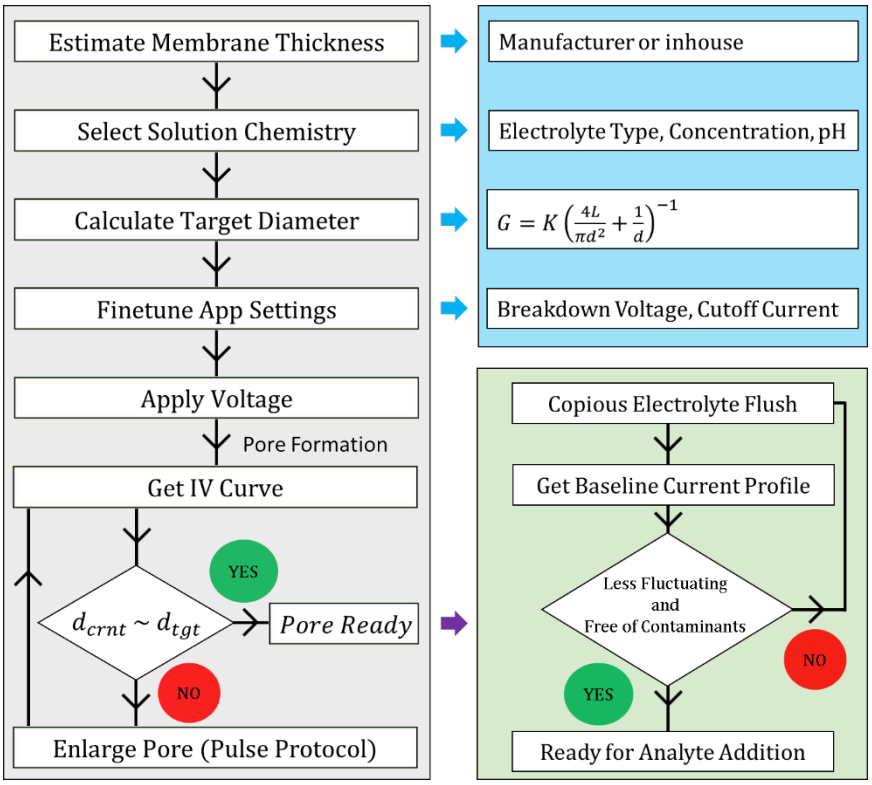

Figure 4: Flow diagram corresponding to pore fabrication. Black arrows indicate the flow of the process, while blue arrows indicate the parameters governing each corresponding step.

Figure 5a shows a screenshot of the panel where the cutoff current is set based on d_{target}, membrane thickness, electrolyte conductivity, and breakdown voltage. The application calculates the electric field based on these inputs. It warns the user if the electric field exceeds the maximum permissible level of 1 V/nm by changing the bulb's color (next to the *Electric Field V/nm* field) to red. The user can opt to either use 100% of the cutoff current (I_t) or a fraction of it (using *I Fraction* command). By using a fraction of the I_t, a pore with a diameter smaller than the intended d_{target} is favored, which can later be enlarged. The I_t is calculated using equation 1. For example, to form a 6 nm diameter pore through a ~12 nm thick SiN_x membrane using an applied voltage of 6 V submerged in a 1 M KCl with 10.85 S/m conductivity, the I_t would be ~110.1 nA. As seen in Figure 5b, with the application of the electric field, a non-ohmic current is seen, which is attributed to the leakage current, I_L. Afterward, a rapid surge in the

current is seen, which is indicative of pore formation: the voltage application is continued until the current reaches I_t. Before this rapid current surge, with some membranes, we observed a drop in the current (Figure 5c, with more examples shown in Figure S6). This could be due to the fact, with the initial pore formation, the current becomes dominant by Ohmic contributions (i.e., current through the initially formed pore), and given the fact that I_L is typically in the range of a couple of tens of nA; if the initially formed pore is small enough, a noticeable drop in the current from the I_L can be expected. However, we see that the magnitude of this drop in current (with respect to the I_L) is not predictable (i.e., some cases, such as the one shown in Figure 5a, produce no noticeable drop in the current from the I_L before the rapid surge of the current). Those producing a significantly noticeable drop (Figure S6) from the I_L can potentially be used to alert the GUI of the beginning of the formation of a pore. This could have applications for users who would like to stop the voltage application at the first possible instance of a pore formation and then grow it controllably with a lower voltage to a desired size.

To measure the pore size after the initial pore formation (or at any point after the pore formation), the MATLAB application is incorporated with an I-V curve acquisition protocol (measures only in the positive voltage biases), as seen in Figures 5d and 5e. Unlike the I-V curves obtained from the Elements amplifier (Figure S7), the Arduino setup can only capture current information in the positive voltage bias. This is because Arduino boards typically cannot apply negative voltages, and the external ADC used in this design can only measure down to 0.3V below the ground. Although the positive voltage bias-based I-V curves work well for high salt conditions where rectification is typically negligible, it (i.e., the Arduino device) would not perform well under conditions where current rectification is not insignificant. A comparison of conductance calculated from this I-V curve protocol with that from the Elements amplifier revealed a close agreement between the two readouts, as seen in Figure 5f. It is worth noting that the I-V acquisition with the external DAC yields values closer to the ideally anticipated value than the PWM-OP-AMP module, as seen in Figure 5f. This is unsurprising since the external DAC produces a less noisy

voltage output (Figure 2a). Additionally, the external DAC is a 12-bit module (PWM-OP-AMP is 8-bit), which would result in higher-resolution readouts with the former.

If the pore size is much smaller than anticipated, we have incorporated a voltage pulse protocol to grow the pore (Figure 5g). With this, a higher voltage pulse is applied over a pre-determined time to grow the pore, followed by a lower voltage pulse (typically 0.2-0.5V) to measure the size of the pore, as shown in Figure 5h. If needed, the MATLAB application can estimate the pore size using the current at both or either higher or lower voltage pulse segments. The pore shown in Figure 5h had an initial size of ~8.7 nm (membrane thickness ~12 nm). Then, it was grown with a high voltage pulse of 8 V lasting 2 s and a low pulse of 0.5 V lasting 5 s (for demonstration purposes only). After six pulses, the pore diameter was estimated to be ~10.3 nm (target was ~10 nm). Another example is shown in Figure 5i, where an initially ~2.6 nm diameter pore through a ~10 nm thick membrane was enlarged to ~3.9 nm (target was ~5 nm) using alternating voltage pulses of 6 V (2 seconds) and 0.5 V (5 seconds).

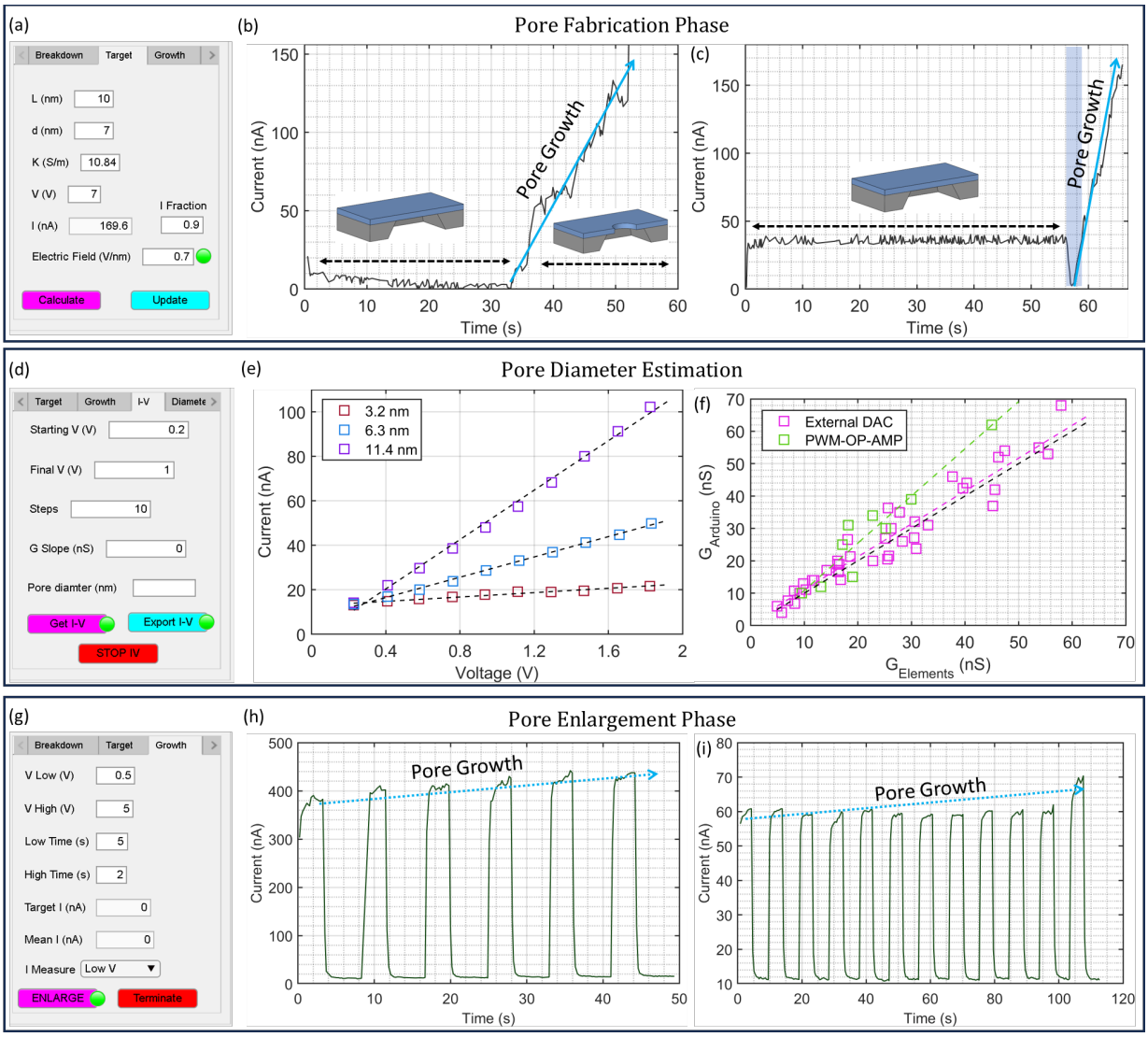

Figure 5: (**a**) Screenshot of the panel with target diameter and applied voltage commands to determine the cutoff current. **(b)** and **(c)** Current traces for fabricating ~6.4 nm and ~5.9 nm diameter pores (through ~10 nm and ~12 nm thick SiN_x membranes, respectively) under an electric field of 0.6 V/nm and 0.75 V/nm, respectively. The rapid current surge indicates pore formation and its subsequent growth. **(d)** Screenshot of the panel with commands for I-V curve acquisition to estimate the pore diameter. **(e)** I-V curves from the Arduino setup correspond to ~3.2 nm, 6.3 nm, and 11.4 nm diameter pores. The pore sizes estimated from the I-V curves were ~2.9 nm, ~6.8 nm, and ~11.8 nm, respectively. **(f)** Estimating the pore diameter using the I-V protocol of the Arduino device with PWM-OP-AMP module (green

squares; n=9) and 12-bit external DAC (magenta squares; n=40) for voltage application. The dashed line in blue represents the ideally expected relationship (i.e., slope =1). In contrast, the magenta and green dashed lines represent linear fits to the data obtained with a 12-bit external DAC and PWM-OP-AMP module, respectively. **(g)** Screenshot of the panel with commands pore enlargement protocol. **(h)** Enlargement of an initially ~8.7 nm diameter pore through a ~12 nm thick membrane to ~10.3 nm (target was ~10 nm) using alternating voltage pulses of 8 V (2 seconds) and 0.5 V (5 seconds). **(i)** Enlargement of an initially ~2.6 nm diameter pore through a ~10 nm thick membrane to ~3.9 nm (target was 5 nm) using alternating voltage pulses of 6 V (2 seconds) and 0.5 V (5 seconds).

A total of 60 pores were fabricated using this setup, as seen in Figure 6b: 21 pores were fabricated with the PWM-OP-AMP module, and a further 39 were fabricated using the external DAC (i.e., MCP4725). Table S2 outlines the solution chemistry and voltages used for the fabrication of these 60 pores. We observed no noticeable differences in nanopores fabricated with either voltage application method. Moreover, with this setup, we could conveniently fabricate <5 nm diameter pores: the smallest pore size attempted was ~3 nm. Since smaller pores (in the range of 2 nm) are known to be initially rectifying and require prolonged soaking in higher-molar LiCl solutions,[40] we opted to fabricate pores in size regimes where such soaking was unnecessary. The standard deviation of the baseline ($\sigma_{baseline}$) was used as a measure of pore-noise. The $\sigma_{baseline}$ was estimated using trace obtained in 1M KCl (pH~8; same conditions used for DNA translocation experiments) and was found to be ~99±12 pA (12 pores). The power spectral density (PSD) graphs of 12 pores are shown in Figure S8. The distribution of the difference in the fabricated and target pore diameters (d_{fab} and d_{target} respectively) are shown in Figure 6c. Figure 6d shows the percentage of pores smaller than the deviation represented by the absolute value of $d_{fab} - d_{target}$. As seen by both Figures 6c and 6d, ~80% of the fabricated pores with this setup were within 1 nm of the target diameter. From these pore fabrication results through this device, the following two recommendations are made for the users: 1) for small pore fabrication (<5 nm), it is best to use about 80% of the calculated I_t to

account for pore growth that can take place during the time it takes the software to terminate the voltage application to the nanopore, and 2) for fabrication of pores that are >5 nm in diameter, it is best first to fabricate a ~ 5nm diameter pore and then gradually increase the size.

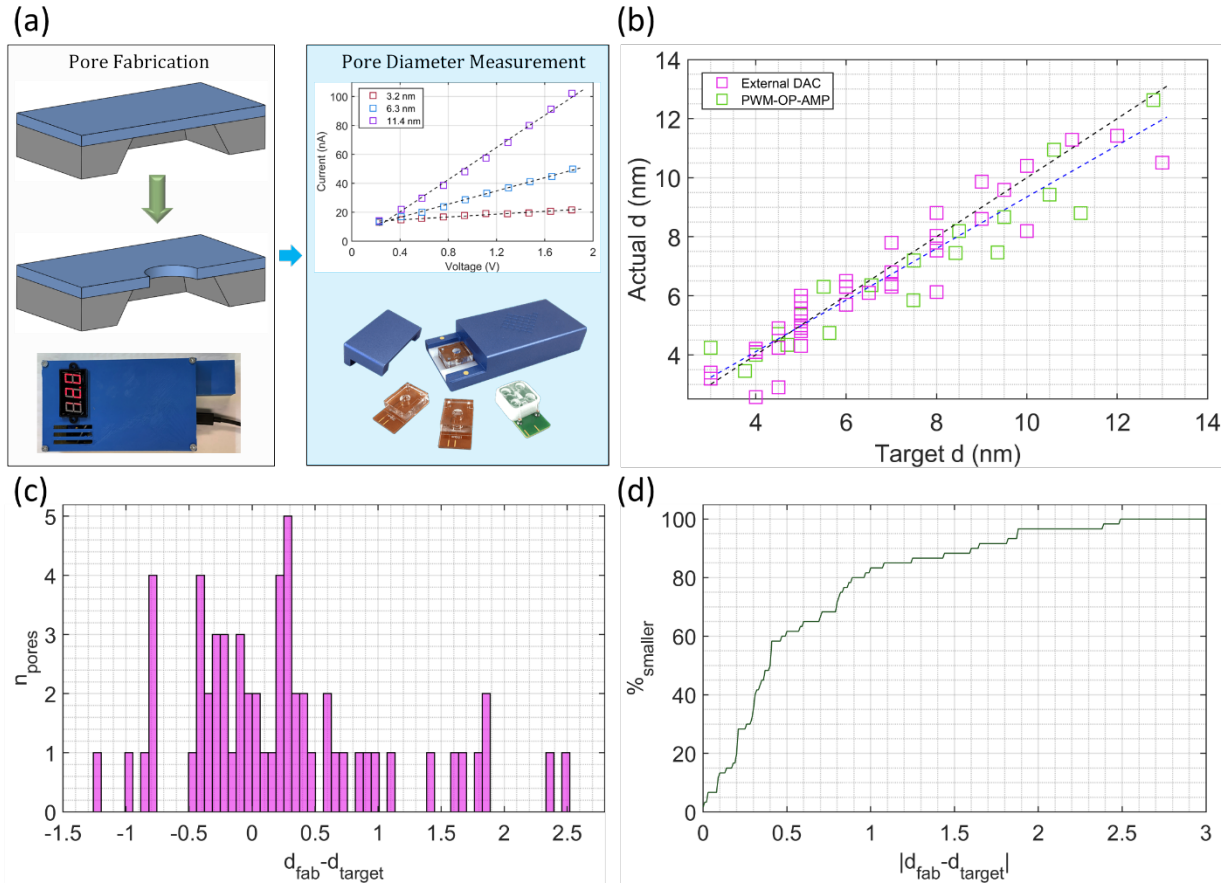

Figure 6: **(a)** After fabricating a pore using the Arduino setup, the flowcell sandwiching the nanopore is transferred to the Elements Amplifier to calculate the actual pore diameter with the aid of equation 1 (image copyrights of the Elements amplifier exclusively belongs to *ELEMENTS SRL*). **(b)** A plot of actual vs. target pore diameters (n=60) with PWM-OP-AMP module (green squares; n=21) and 12-bit external DAC (magenta squares; n=39) for voltage application. The black dashed line represents the ideally expected value (i.e., slope =1). In contrast, the blue represents a linear fit to the diameter of pores fabricated with the Arduino device (only as a guide to the eye). **(c)** The distribution of the difference in

fabricated and target pore diameters (d_{fab} and d_{target} respectively). **(d)** A plot depicting the percentage of pores smaller ($\%_{small}$) than the deviation represented by the absolute value of $d_{fab} - d_{target}$.

DNA Translocation

To see whether the fabricated pores are suitable for single-molecule translocation experiments, we used a 1 kb double-stranded DNA (dsDNA) ladder. The dsDNA was added to the *cis* side (i.e., grounded side) and driven across the membrane in response to a positive bias (+ 400mV) applied to the *trans* side. For this, ~4.3 nm and ~8.8 nm diameter pores were used, as shown in Figures 7b and 7c. A total of 2,428 and 15,739 events (respectively) were collected from these two pores, which are comparable with that collected typically with pores fabricated via CBD technology.[25] While it is possible to collect more events, the purpose of this study was to show that the pores fabricated using the Arduino device using the CBD protocol are conducive for translocation experiments. Moreover, the translocation characteristics resemble those observed with pores fabricated with CBD technology. As expected, translocations through the smaller pore yielded a higher blockage percentage. For ease of comparison, identical scales were adopted for the scatter plots in Figures 7d and 7e. Translocation of dsDNA through the ~4.3 nm diameter shown in Figure 5 yielded a conductance change (ΔG_{dsDNA}) of ~6.9 nS. Using the dynamic cross section of the B-form of dsDNA (2.2 nm), the effective diameter and length were calculated to be ~4.0 nm and ~11.9 nm, respectively. The membrane thickness calculated using ellipsometry for this membrane was ~12 ± 2 nm, which is in good agreement with that calculated ΔG_{dsDNA}.

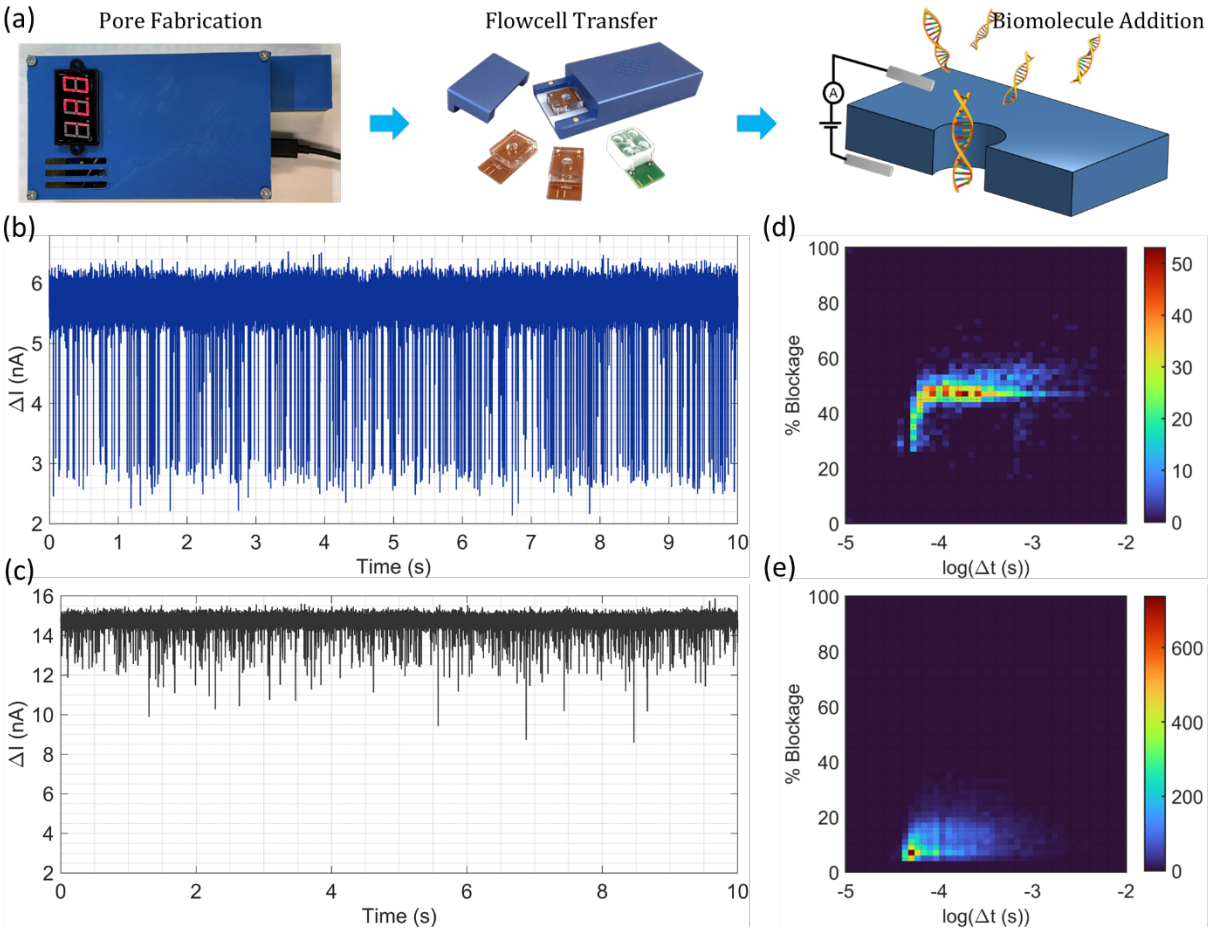

Figure 7: (a) After fabricating a pore using the Arduino setup, the flowcell sandwiching the nanopore is transferred to the Elements Amplifier (image copyrights of the Elements amplifier exclusively belongs to *ELEMENTS SRL*) after which the biomolecule of interest (DNA in this case) is added to the cis side and a suitable voltage bias is applied to the trans side (+400 mV in this case) to drive the biomolecule across the nanopore. **(b)** and **(c)** 10-second current traces corresponding to DNA translocation through ~3.7 nm and ~8.8 nm diameter pores, respectively. The respective scatter plots (blockage percentage vs log of the dwell time) are shown in **(d)** and **(e)**. A total of 2,428 and 15,739 events were recorded with these pores, respectively. All experiments used 1M KCl buffered at pH ~7 under an applied voltage bias of +400 mV.

While our device-app combination delivers a host of features, we note the following could further improve the design:

i) Implementation of the application in an open-source platform.

ii) Use of a Faraday cage to house the flowcell.

iii) Improving the noise characteristics for the fabrication of ultra-small pores (i.e., <2 nm)

iv) Grounding the Arduino to have all readings referenced to a true ground (might not be practical in portable applications).

v) Increasing the data acquisition rate. The I^2C protocol of MATLAB has many back-and-forths, which slows the data transmission compared to the native Arduino IDE platform. Serial communication could be an alternative where MATLAB would function to fetch the serial readouts, and the device would be programmed solely through the native Arduino IDE.

vi) Although not implemented in the current design, we have noticed the current values to be more stable when the connection point of the nanopore and the feedback resistor of OP-AMP #2 are grounded through a 100 nF capacitor.

Concluding Remarks

In this work, we have demonstrated a highly-performing device design for nanopore fabrication via CBD, costing less than 150 USD. All components used to build the device are readily available through mainstream global retailers. The device is powered through the same USB cable used to communicate with the PC, which emboldens its portability. Using this device, we fabricated nanopores via the CBD technique through Si-rich silicon nitride membranes. Pores ranging from ~2.5 nm to 12.6 nm in diameter were fabricated, with ~80% of the pores within 1 nm of the intended target diameter. The initially fabricated pores were slightly smaller than the target diameter and were enlarged using the alternating high-low voltage-pulse cycle method built into the MATLAB app. This device can conveniently fabricate pores in the coveted <5 nm diameter range. Most importantly, the device is portable, and together with the portable

amplifier used for translocation experiments, it creates a holistically portable experimental setup suited for on-field applications. With research efforts to develop low-cost amplifiers, our Arduino-based device enabling membrane fabrication and nanopore sensing provides a portable, accessible, low-cost technology with broad application potential from pore fabrication to simple resistance measurements.

Acknowledgments

YMNDYB, BIK, AT, and PK were supported by the ANU Grand Challenge '*Our Health in Our Hands*'. SD was supported by an AINSE Ltd. Postgraduate Research Award (PGRA) and the Australian Government Research Training Program (RTP) Scholarship. AT also acknowledges financial support from the Australian Research Council (ARC) Future Fellowship Scheme (FT200100939), ARC Discovery Project Scheme (DP190101864), and National Intelligence and Security Discovery Research Grant (NS210100083). AT would also like to acknowledge the North Atlantic Treaty Organization – Science for Peace and Security Program: "*Advanced Metal Oxides and Heterostructures for Electro-optical Chemical Sensors*" and Ramaciotti Foundation: "*Demonstrating detection of validated and candidate relapse indicators of MS using a first in class portable device*". PK also acknowledges financial support from the ARC Discovery Project Scheme (DP180100068).

Disclaimers

The authors declare no competing financial interests.

Data Availability

The data that support the findings of this study are available from the corresponding author upon reasonable request.

References

1. Lastra, L. S.; Bandara, Y.; Nguyen, M.; Farajpour, N.; Freedman, K. J., On the origins of conductive pulse sensing inside a nanopore. *Nature Communications* **2022,** *13* (1), 1-11.

2. Bandara, Y. N. D.; Freedman, K. J., Enhanced Signal to Noise Ratio Enables High Bandwidth Nanopore Recordings and Molecular Weight Profiling of Proteins. *ACS Nano* **2022,** *16* (9), 14111-14120.
3. Karawdeniya, B. I.; Bandara, Y. M. N. D. Y.; Khan, A. I.; Chen, W. T.; Vu, H.-A.; Morshed, A.; Suh, J.; Dutta, P.; Kim, M. J., Adeno-associated virus characterization for cargo discrimination through nanopore responsiveness. *Nanoscale* **2020,** *12* (46), 23721-23731.
4. Karawdeniya, B. I.; Bandara, Y. N. D.; Nichols, J. W.; Chevalier, R. B.; Dwyer, J. R., Surveying silicon nitride nanopores for glycomics and heparin quality assurance. *Nature Communications* **2018,** *9* (1), 3278.
5. Freedman, K. J.; Haq, S. R.; Edel, J. B.; Jemth, P.; Kim, M. J., Single molecule unfolding and stretching of protein domains inside a solid-state nanopore by electric field. *Scientific Reports* **2013,** *3*, 1638.
6. Lin, C.-Y.; Fotis, R.; Xia, Z.; Kavetsky, K.; Chou, Y.-C.; Niedzwiecki, D. J.; Biondi, M.; Thei, F.; Drndić, M., Ultrafast Polymer Dynamics through a Nanopore. *Nano Letters* **2022**.
7. Kasianowicz, J. J.; Brandin, E.; Branton, D.; Deamer, D. W., Characterization of individual polynucleotide molecules using a membrane channel. *Proceedings of the National Academy of Sciences* **1996,** *93* (24), 13770-13773.
8. Bezrukov, S. M.; Vodyanoy, I.; Parsegian, V. A., Counting polymers moving through a single ion channel. *Nature* **1994,** *370* (6487), 279-281.
9. Li, N.; Yu, S.; Harrell, C. C.; Martin, C. R., Conical nanopore membranes. Preparation and transport properties. *Analytical Chemistry* **2004,** *76* (7), 2025-2030.
10. Siwy, Z.; Fuliński, A., A nanodevice for rectification and pumping ions. *American Journal of Physics* **2004,** *72* (5), 567-574.
11. Mara, A.; Siwy, Z.; Trautmann, C.; Wan, J.; Kamme, F., An asymmetric polymer nanopore for single molecule detection. *Nano Letters* **2004,** *4* (3), 497-501.
12. Li, J.; Stein, D.; McMullan, C.; Branton, D.; Aziz, M. J.; Golovchenko, J. A., Ion-beam sculpting at nanometre length scales. *Nature* **2001,** *412* (6843), 166-169.
13. Qiu, H.; Zhou, W.; Guo, W., Nanopores in Graphene and Other 2D Materials: A Decade's Journey toward Sequencing. *ACS Nano* **2021,** *15* (12), 18848-18864.
14. Merchant, C. A.; Healy, K.; Wanunu, M.; Ray, V.; Peterman, N.; Bartel, J.; Fischbein, M. D.; Venta, K.; Luo, Z.; Johnson, A. T. C.; Drndić, M., DNA Translocation through Graphene Nanopores. *Nano Letters* **2010,** *10* (8), 2915-2921.
15. Saharia, J.; Bandara, Y. N. D.; Lee, J. S.; Wang, Q.; Kim, M. J.; Kim, M. J., Fabrication of hexagonal boron nitride based 2D nanopore sensor for the assessment of electro-chemical responsiveness of human serum transferrin protein. *Electrophoresis* **2020,** *41* (7-8), 630-637.
16. Alibakhshi, M. A.; Kang, X.; Clymer, D.; Zhang, Z.; Vargas, A.; Meunier, V.; Wanunu, M., Scaled-up synthesis of freestanding molybdenum disulfide membranes for nanopore sensing. *Advanced Materials* **2023,** *35* (12), 2207089.
17. Graf, M.; Liu, K.; Sarathy, A.; Leburton, J.-P.; Radenovic, A., Transverse Detection of DNA in a MoS_2 Nanopore. *Nature Nanotechnology* **2015,** *10*, 1070-1077.
18. Danda, G.; Masih Das, P.; Chou, Y.-C.; Mlack, J. T.; Parkin, W. M.; Naylor, C. H.; Fujisawa, K.; Zhang, T.; Fulton, L. B.; Terrones, M., Monolayer WS2 nanopores for DNA translocation with light-adjustable sizes. *ACS Nano* **2017,** *11* (2), 1937-1945.
19. Larkin, J.; Henley, R.; Bell, D. C.; Cohen-Karni, T.; Rosenstein, J. K.; Wanunu, M., Slow DNA transport through nanopores in hafnium oxide membranes. *ACS Nano* **2013,** *7* (11), 10121-10128.
20. Zhu, L.; Liu, Y.; Zhao, Y.; Yan, H.; Wang, Q.; Pei, R., Discrimination of Short ssDNA Using Nanopore-Fabricated Self-Assembled Metal–Organic Framework Membranes. *ACS Applied Nano Materials* **2022,** *5* (12), 18581-18590.

21. Wang, R.; Gilboa, T.; Song, J.; Huttner, D.; Grinstaff, M. W.; Meller, A., Single-molecule discrimination of labeled DNAs and polypeptides using photoluminescent-free TiO2 nanopores. *ACS Nano* **2018,** *12* (11), 11648-11656.
22. Park, K.-B.; Kim, H.-J.; Kang, Y.-H.; Yu, J.-S.; Chae, H.; Lee, K.; Kim, H.-M.; Kim, K.-B., Highly reliable and low-noise solid-state nanopores with an atomic layer deposited ZnO membrane on a quartz substrate. *Nanoscale* **2017,** *9* (47), 18772-18780.
23. Kim, M. J.; Wanunu, M.; Bell, D. C.; Meller, A., Rapid fabrication of uniformly sized nanopores and nanopore arrays for parallel DNA analysis. *Advanced Materials* **2006,** *18* (23), 3149-3153.
24. Yang, J.; Ferranti, D. C.; Stern, L. A.; Sanford, C. A.; Huang, J.; Ren, Z.; Qin, L.-C.; Hall, A. R., Rapid and precise scanning helium ion microscope milling of solid-state nanopores for biomolecule detection. *Nanotechnology* **2011,** *22* (28), 285310.
25. Kwok, H.; Briggs, K.; Tabard-Cossa, V., Nanopore fabrication by controlled dielectric breakdown. *PLoS One* **2014,** *9* (3), e92880.
26. Ying, C.; Houghtaling, J.; Eggenberger, O. M.; Guha, A.; Nirmalraj, P.; Awasthi, S.; Tian, J.; Mayer, M., Formation of single nanopores with diameters of 20–50 nm in silicon nitride membranes using laser-assisted controlled breakdown. *ACS Nano* **2018,** *12* (11), 11458-11470.
27. Yanagi, I.; Akahori, R.; Hatano, T.; Takeda, K., Fabricating nanopores with diameters of sub-1 nm to 3 nm using multilevel pulse-voltage injection. *Scientific Reports* **2014,** *4*, 5000.
28. Zhang, Y.; Miyahara, Y.; Derriche, N.; Yang, W.; Yazda, K.; Capaldi, X.; Liu, Z.; Grutter, P.; Reisner, W., Nanopore Formation via Tip-Controlled Local Breakdown Using an Atomic Force Microscope. *Small Methods* **2019,** *3* (7), 1900147.
29. Arcadia, C. E.; Reyes, C. C.; Rosenstein, J. K., In situ nanopore fabrication and single-molecule sensing with microscale liquid contacts. *Acs Nano* **2017,** *11* (5), 4907-4915.
30. Bandara, Y. N. D.; Karawdeniya, B. I.; Dwyer, J. R., Push-Button Method To Create Nanopores Using a Tesla-Coil Lighter. *ACS Omega* **2019,** *4* (1), 226-230.
31. Saharia, J.; Bandara, Y. M. N. D. Y.; Karawdeniya, B. I.; Dwyer, J. R.; Kim, M. J., Over One Million DNA and Protein Events Through Ultra-Stable Chemically-Tuned Solid-State Nanopores. *Small* **2023**, 2300198.
32. D. Y. Bandara, Y. M. N.; Saharia, J.; Karawdeniya, B. I.; Hagan, J. T.; Dwyer, J. R.; Kim, M. J., Beyond nanopore sizing: improving solid-state single-molecule sensing performance, lifetime, and analyte scope for omics by targeting surface chemistry during fabrication. *Nanotechnology* **2020,** *31* (33), 335707.
33. Dutt, S.; Karawdeniya, B. I.; Bandara, Y. N. D.; Afrin, N.; Kluth, P., Ultrathin, High-Lifetime Silicon Nitride Membranes for Nanopore Sensing. *Analytical Chemistry* **2023,** *95* (13), 5754-5763.
34. Wang, Y.; Chen, Q.; Deng, T.; Liu, Z., Nanopore fabricated in pyramidal HfO2 film by dielectric breakdown method. *Applied Physics Letters* **2017,** *111* (14), 143103.
35. Zhang, X.; van Deursen, P. M.; Fu, W.; Schneider, G. g. F., Facile and ultraclean graphene-on-glass nanopores by controlled electrochemical etching. *ACS Sensors* **2020,** *5* (8), 2317-2325.
36. Feng, J.; Liu, K.; Graf, M.; Lihter, M.; Bulushev, R. D.; Dumcenco, D.; Alexander, D. T.; Krasnozhon, D.; Vuletic, T.; Kis, A., Electrochemical reaction in single layer MoS2: nanopores opened atom by atom. *Nano Letters* **2015,** *15* (5), 3431-3438.
37. Leung, C.; Briggs, K.; Laberge, M.-P.; Peng, S.; Waugh, M.; Tabard-Cossa, V., Mechanisms of solid-state nanopore enlargement under electrical stress. *Nanotechnology* **2020,** *31* (44), 44LT01.
38. Goto, Y.; Yanagi, I.; Matsui, K.; Yokoi, T.; Takeda, K.-i., Integrated solid-state nanopore platform for nanopore fabrication via dielectric breakdown, DNA-speed deceleration and noise reduction. *Scientific Reports* **2016,** *6*, 31324.
39. Briggs, K.; Charron, M.; Kwok, H.; Le, T.; Chahal, S.; Bustamante, J.; Waugh, M.; Tabard-Cossa, V., Kinetics of nanopore fabrication during controlled breakdown of dielectric membranes in solution. *Nanotechnology* **2015,** *26* (8), 084004.

40. Briggs, K.; Kwok, H.; Tabard-Cossa, V., Automated fabrication of 2-nm solid-state nanopores for nucleic acid analysis. *Small* **2014,** *10* (10), 2077-2086.
41. Waugh, M.; Briggs, K.; Gunn, D.; Gibeault, M.; King, S.; Ingram, Q.; Jimenez, A. M.; Berryman, S.; Lomovtsev, D.; Andrzejewski, L., Solid-state nanopore fabrication by automated controlled breakdown. *Nature Protocols* **2020,** *15* (1), 122-143.
42. St-Denis, T.; Yazda, K.; Capaldi, X.; Bustamante, J.; Safari, M.; Miyahara, Y.; Zhang, Y.; Grutter, P.; Reisner, W., An apparatus based on an atomic force microscope for implementing tip-controlled local breakdown. *Review of Scientific Instruments* **2019,** *90* (12), 123703.
43. Fang, S.; Yin, B.; Xie, W.; Zhou, D.; Tang, P.; He, S.; Yuan, J.; Wang, D., A novel dielectric breakdown apparatus for solid-state nanopore fabrication with transient high electric field. *Review of Scientific Instruments* **2020,** *91* (9), 093203.
44. Kuan, A. T.; Lu, B.; Xie, P.; Szalay, T.; Golovchenko, J. A., Electrical pulse fabrication of graphene nanopores in electrolyte solution. *Applied Physics Letters* **2015,** *106* (20), 203109.
45. Bandara, Y. N. D.; Saharia, J.; Karawdeniya, B. I.; Kluth, P.; Kim, M. J., Nanopore Data Analysis: Baseline Construction and Abrupt Change-Based Multilevel Fitting. *Analytical Chemistry* **2021,** *93* (34), 11710-11718.